Transport of a wave packet through nanostructures: Quantum kinetics of carrier capture processes

M. Glanemann, V. M. Axt, and T. Kuhn
Institut für Festkörpertheorie, Westfälische Wilhelms–Universität Münster, Wilhelm-Klemm-Strasse 10, 48149, Münster, Germany
(Received 24 March 2005; published 22 July 2005)

Capture processes of an electronic wave packet traveling in a quantum wire into localized states of an embedded quantum dot by means of phonon emission are studied in a quantum kinetic approach. It turns out that due to the ultrashort length and time scales involved the capture processes exhibit a variety of quantum kinetic features which cannot be described by a simple semiclassical capture rate. We find in general a nonmonotonic rise of the occupation of bound states even at low temperatures where no phonon absorption is possible. This is related to the finite collision duration and the presence of coherent superpositions between initial and final states in the scattering process giving rise to phonon Rabi oscillations between free and trapped states. In the case of more than one bound state in the dot typically a linear combination of these bound states is populated, which leads to a nontrivial dynamics of the trapped carrier density. For potential profiles with large reflection probability it turns out that also the transmission and reflection behavior is modified by the capture process. Finally the theory is applied to a two-band model including optical excitation and excitonic effects. For the scenarios studied in the paper these phenomena lead to some quantitative modifications but they do not change the characteristic quantum features of the capture dynamics.

DOI: 10.1103/PhysRevB.72.045354 PACS number(s): 73.63.−b, 78.67.−n, 72.20.Jv, 72.10.Di

I. Introduction

Due to the continuous reduction of length and time scales in modern nano- and optoelectronic structures and devices the carrier dynamics in these systems is increasingly governed by quantum mechanical features. The basic assumptions inherent in the semiclassical kinetic theory, i.e., the separation of the dynamics into sequences of free flights, where the carriers are accelerated by the effective local electric field, and scattering processes which occur pointlike in space and time between states with well-defined momentum and energy, lose their validity. For the description of both transport processes and optical properties a quantum kinetic approach is needed which overcomes the limitations of semiclassical kinetics.[1,2]

Carriers moving in potential profiles varying on a nanometer scale do not behave anymore like classical particles which are accelerated according to the local potential gradient. This deterministic behavior is complemented by a stochastic aspect given by the quantum mechanical probabilities for reflection and transmission. Furthermore such profiles may change the spectral characteristics of the carriers by introducing a discrete part in the energy spectrum associated with localized states. Besides the modifications of the ballistic part (free flights) of the dynamics also the description of scattering processes has to be changed. In particular in the presence of localized states the notion of a local scattering process between states with well-defined momenta does not make sense anymore because these localized states do not have well-defined momenta. This problem can be overcome by calculating scattering rates between the states defined by the potential, which is of course successfully done in the modeling of carrier transport in low-dimensional structures like quantum wells and quantum wires. Difficulties arise, however, if scattering processes between states with different effective dimensionalities are considered, such as capture processes from delocalized states into localized states. In this case the scattering rates typically depend on the normalization volume of the delocalized states which then has to be fixed by some more or less rigorous argument. This behavior is related to the fact that as long as only occupations are considered, as is often done in these calculations, the electrons that occupy continuum states are always completely delocalized. Spatially inhomogeneous distributions where the carriers are not completely delocalized require superpositions of these states and therefore off-diagonal elements in the density matrices defined with respect to these states.

Examples for such capture processes into states with lower dimension are abundant in modern micro- and nanostructured devices. In a quantum well laser carriers have to be trapped from the three-dimensional transport states into the two-dimensional states in the active region. In the case of self-assembled quantum dots carriers are often generated optically in the two-dimensional wetting layer states from which they are trapped into the zero-dimensional quantum dot states. Also combined quantum wire–quantum dot structures have been fabricated either by cleaved-edge overgrowth[3] or by growth on a patterned substrate.[4] In these structures carriers may undergo transitions between one-dimensional quantum wire states and zero-dimensional quantum dot states. In the present paper we will address such a capture from quasi-one-dimensional into quasi-zero-dimensional states. Because of their importance for heterostructure semiconductor lasers capture rates obtained from Fermi's golden rule have been calculated for many years, first mainly for the capture into quantum well states[5–9] and more recently also for the capture into quantum dot states.[10–13] In contrast to such a golden rule treatment, in this paper we present a quantum kinetic description which accounts for quantum coherences during the scattering process

as well as the fundamental quantum mechanical uncertainties.

Another source of ultrashort length scales in the carrier dynamics is a localized optical excitation. By exciting the sample through the tip of a near-field optical microscope[14–16] spot sizes down to a few tens of nanometers have been achieved.[17] These techniques have been applied, e.g., to the study of exciton transport[15] and to selective excitations in structured samples including quantum wells, wires, and dots.[4,16] Various aspects of the spatiotemporal dynamics of strongly localized electronic and excitonic wave packets have been studied theoretically mainly by using a density matrix formalism. These include the role of the Coulomb interaction and light field coupling[18,19] and the influence of carrier-phonon interaction which has been treated either in the Markov approximation[20] or in a quantum kinetic approach.[21,22]

Besides ultrashort length scales also ultrashort time scales lead to a failure of the semiclassical theory. The assumption of instantaneous scattering processes between states with well-defined energies is not compatible with the fundamental uncertainty between energy and time. The limitations of a semiclassical kinetic theory which are reached when reducing length and/or time scales are overcome by a quantum kinetic theory.[1,2,23] A variety of quantum kinetic phenomena on ultrashort time scales has been studied in recent years both theoretically and experimentally. Most of the investigations have been performed on spatially homogeneous systems.[24–31] More recently, the quantum kinetic theory has also been applied to spatially inhomogeneous systems.[21] In quantum dot structures the ultrafast initial decoherence of the optical polarization has been found to be essentially related to pure dephasing, i.e., to interaction processes without real transitions between electronic states, which results in a genuinely non-Markovian dynamics and non-Lorentzian spectra.[32–34] In the case of transport of strongly localized wave packets energy-nonconserving transitions may lead to an additional spatial broadening of the wave packet.[21]

In this paper we will study the dynamics of carrier transport and capture processes in a quantum kinetic approach. To be specific, we will assume that the carriers are initially prepared as a localized traveling wave packet in a semiconductor quantum wire, e.g., by means of an ultrafast optical excitation through the tip of a near-field optical microscope. This wave packet then approaches a quantum dot embedded in the wire and, due to the interaction with longitudinal optical phonons, may undergo transitions from the initial delocalized continuum states into localized bound states. Therefore, the present scenario combines the aspects of ultrashort length scales both in the initial carrier distribution and in the potential profile with the ultrashort time scales introduced by the optical excitation. It will turn out that the question of the final state reached after a capture process is by no means a trivial one. Hence it is of particular importance that the quantum kinetic treatment is independent of the basis chosen for the dynamical variables, in contrast to the semiclassical description which requires an *a priori* knowledge of the final state of a scattering process.

The scenario we are studying introduces another fascinating aspect. By exciting the wave packet in the quantum wire region below the threshold for LO phonon emission and considering the case of low temperatures, the electron-phonon interaction is effectively switched on only when the wave packet reaches the dot region. Furthermore, for the traveling part the interaction is switched off again when the wave packet leaves the dot region. This is somewhat similar to the case of an atom flying through a microcavity where the interaction with the light field is also present only as long as the atom is inside the cavity.[35] Indeed we observe in the carrier dynamics signatures of carrier-phonon Rabi oscillations in analogy with atom-photon Rabi oscillations in a microcavity. The short effective duration of the carrier-phonon interaction gives rise to another phenomenon which is similar to the carrier-light interaction in the case of a short laser pulse. It turns out that the carrier-phonon interaction may create electronic quantum beats between different localized quantum dot states similar to the creation of electronic quantum beats after ultrafast optical excitation.

The paper is organized as follows. In Sec. II we will briefly review the density matrix approach to quantum kinetics for spatially inhomogeneous systems. Here we will compare different representations and address the question of the most suitable basis for numerical implementations. Section III is then devoted to numerical results for various combinations of system parameters and initial or excitation conditions. We will start with sufficiently smooth potentials where essentially no reflection occurs and compare potential profiles with different numbers of bound states. Then we will consider the case of square well potentials which in certain energy ranges exhibit a noticeable probability for reflection of the incident carriers. Here the main focus will be the question of how the transmission and reflection properties of the potential profiles are modified by capture processes. Finally we will extend our analysis to a two-band model. This will allow us to treat consistently the optical excitation by a short and spatially localized laser pulse and thus to model in a more realistic way possible experimental scenarios. In Sec. IV we will summarize our results and draw some conclusions.

II. Theory

In this paper we will study capture processes in both a one-band and a two-band model. The two-band model includes the optical generation of carriers by means of a short laser pulse. In order to describe realistically the coupling of a light field to a semiconductor in the region close to the band edge it is essential to include also the Coulomb interaction at least on the mean-field level to describe excitonic effects and the Coulomb-induced modifications of the oscillator strength of band-to-band continuum transitions. The one-band model is obtained from the two-band model by switching off the carrier-light and Coulomb interaction and neglecting the hole dynamics. The full Hamiltonian for our system as well as a detailed derivation and discussion of the quantum kinetic equations of motion in the density matrix approach both in momentum and Wigner representation can be found in Ref. 21. While in a homogeneous system these density matrices are diagonal in a crystal momentum (**k**-space) representation,

in an inhomogeneous system also the off-diagonal elements are nonvanishing. The basic electronic variables in the two-band model are therefore the single-particle density matrices for electrons f^e and for holes f^h, and the interband density matrix p defined as

$$f^e_{\mathbf{k}',\mathbf{k}} = \langle c^\dagger_{\mathbf{k}'} c_{\mathbf{k}} \rangle, \quad f^h_{\mathbf{k}',\mathbf{k}} = \langle d^\dagger_{\mathbf{k}'} d_{\mathbf{k}} \rangle, \quad p_{\mathbf{k}',\mathbf{k}} = \langle d_{-\mathbf{k}'} c_{\mathbf{k}} \rangle, \quad (1)$$

where $c^\dagger_{\mathbf{k}}$ and $d^\dagger_{\mathbf{k}}$ ($c_{\mathbf{k}}$ and $d_{\mathbf{k}}$) describe the creation (annihilation) of an electron and a hole with momentum $\mathbf{k}$, respectively.

Besides the momentum representations other representations may be used and indeed may be more convenient for specific purposes. One possibility is the Wigner representation. The Wigner functions of electrons and holes are defined as

$$\mathcal{F}^{e,h}_{\mathbf{k}}(\mathbf{r}) = \sum_{\mathbf{q}} e^{i\mathbf{q}\cdot\mathbf{r}} f^{e,h}_{\mathbf{k}-\mathbf{q}/2,\mathbf{k}+\mathbf{q}/2}. \quad (2)$$

This function has the strongest analogy with a classical distribution function. In the one-band model calculations we will use the Wigner representation to define an initial condition. The semiclassical Boltzmann equation for a space-dependent distribution function can be obtained by transforming the equations of motion to the Wigner representation and performing a Markov approximation under the assumption of sufficiently slow spatial and temporal variations. Such a Markov approximation, however, always implies an *a priori* selection of the basis and therefore the resulting semiclassical equations of motion are no longer independent of the basis. A detailed discussion of this aspect including a comparison between different types of Markov approximations can be found in Ref. 21. The full quantum kinetic theory, on the other hand, is completely independent of the choice of the single-particle basis. Therefore, the basis may be selected according to its convenience for practical calculations.

Here we are interested in the dynamics in the the presence of a confinement potential $V^{e,h}(\mathbf{r})$ for electrons and holes. In this case a natural basis is given by the eigenfunctions corresponding to these potentials which are solutions of the time-independent Schrödinger equations for electrons and holes,

$$\left[-\frac{\hbar^2}{2m^{e,h}}\Delta + V^{e,h}(\mathbf{r}) \right] \varphi^{e,h}_n(\mathbf{r}) = \epsilon^{e,h}_n \varphi^{e,h}_n(\mathbf{r}). \quad (3)$$

Here, $m^{e,h}$ are the effective masses of electrons and holes, $\varphi^{e,h}_n(\mathbf{r})$ are the single-particle wave functions, and $\epsilon^{e,h}_n$ are the corresponding single-particle energies. In general, for the problems studied here the single-particle spectrum is partially discrete (for the bound states) and partially continuous (for the delocalized states). Therefore this representation is particularly transparent for the study of transitions between delocalized and localized states, i.e., the carrier capture processes which are at the focus of the present paper.

The basic variables in this representation are the electron density matrix $\rho^e_{n',n}$, the hole density matrix $\rho^h_{n',n}$, and the interband density matrix $p_{n',n}$ which are defined as

$$\rho^e_{n',n} = \langle c^\dagger_{n'} c_n \rangle, \quad \rho^h_{n',n} = \langle d^\dagger_{n'} d_n \rangle, \quad p_{n',n} = \langle d_{n'} c_n \rangle, \quad (4)$$

where $c^\dagger_n$ and $d^\dagger_n$ (c_n and d_n) denote the creation (annihilation) of an electron and a hole in the nth eigenstate $\varphi^{e,h}_n$ of the single-particle Hamiltonian. These density matrices are related to the respective $\mathbf{k}$-space density matrices by a unitary transformation which reads, e.g., for ρ^e:

$$\rho^e_{n',n} = \sum_{\mathbf{k}',\mathbf{k}} \tilde{\varphi}^e_{n'}(\mathbf{k}') \tilde{\varphi}^{e*}_n(\mathbf{k}) f^e_{\mathbf{k}',\mathbf{k}} \quad (5)$$

with the momentum representation of the single-particle eigenstates

$$\tilde{\varphi}^{e,h}_n(\mathbf{k}) = \frac{1}{\sqrt{\mathcal{V}}} \int d^3r\, e^{-i\mathbf{k}\cdot\mathbf{r}} \varphi^{e,h}_n(\mathbf{r}), \quad (6)$$

$\mathcal{V}$ being a normalization volume. Analogously, ρ^e is related to the Wigner function according to

$$\rho^e_{n',n} = \sum_{\mathbf{k},\mathbf{q}} \tilde{\varphi}^e_{n'}\left(\mathbf{k} - \frac{1}{2}\mathbf{q}\right) \tilde{\varphi}^{e*}_n\left(\mathbf{k} + \frac{1}{2}\mathbf{q}\right) \times \frac{1}{\mathcal{V}} \int d^3r\, e^{-i\mathbf{q}\cdot\mathbf{r}} \mathcal{F}^e_{\mathbf{k}}(\mathbf{r}). \quad (7)$$

The equations of motion in this basis have a similar form as in the momentum representation discussed in detail in Ref. 21 [Eqs. (15)–(17)]. When comparing the equations of motion in the $\mathbf{k}$-space representation and in the eigenbasis of the single-particle Hamiltonian one notices that in the latter case the single-particle potential does not appear anymore, but in general the structure is more complicated. The reason is that in the momentum representation both the Coulomb interaction and the electron-phonon interaction are described by coupling matrix elements depending on a single momentum argument. In the eigenbasis the Coulomb matrix elements depend on four electronic indices and the carrier-phonon coupling depends on two electronic indices and the phonon momentum.[23] Therefore the solution of the equations requires more summations to be performed than in the momentum representation. This leads to the question of which representation is better suited for a numerical modeling of the carrier kinetics. Here it turns out that this strongly depends on the system parameters as well as on the excitation or initial conditions for the dynamics. If these conditions are chosen such that only a relatively small energy range is relevant, e.g., by excitation close to the band edge, the eigenbasis is much more convenient because only the states with single-particle energies in this energy range have to be taken into account. In the momentum representation, if spatial variations on short length scales are involved either by a confinement potential or by a strongly localized initial condition, states up to rather high momenta have to be included in order to resolve these short-range spatial variations. Therefore the basis set must be much larger, which makes the numerics less efficient. If, on the other hand, an excitation rather high up in the bands is studied, as has been the case in Ref. 21, the number of states which has to be included is comparable in both representations. In that case the simpler structure of the equations of motion in the momentum representation makes this one favorable for the numeri-

cal implementation. In the present paper we are mainly interested in carrier capture processes. Therefore we will assume excitation conditions close to the band edge such that by the emission of a phonon a localized state in the confinement potential can be reached. In this case the eigenbasis turned out to be much more efficient. In addition we have checked that the calculations in both representations indeed lead to exactly the same results thereby confirming the base independence of the quantum kinetic approach.

III. Results

After having introduced the theoretical approach we will now apply the quantum kinetic theory to capture processes of carriers traveling in a cylindrical GaAs quantum wire with an embedded quantum dot. The carriers are coupled via the Fröhlich interaction to bulk longitudinal optical phonons with an energy of $\hbar\omega_{\mathrm{LO}}=36.4$ meV. The confinement potentials for electrons and holes are taken as the sum of a lateral confinement potential with infinitely high barriers modeling the quantum wire and a longitudinal potential $V^{e,h}(z)$ describing the embedded quantum dot. The eigenstates of the single-particle potential then factorize into a lateral part given by a Bessel function and the eigenfunction $\varphi_n^{e,h}(z)$ of the longitudinal potential. In the lateral direction we will consider only the lowest eigenmode of a cylindrical quantum wire with 100 nm^2 cross section, which therefore reduces the problem to an effectively one-dimensional system. In the longitudinal direction we take periodic boundary conditions with a periodicity length that is sufficiently large such that during the simulation time the boundaries are not reached by the wave packets. In this paper we will restrict ourselves to rather low excitation densities. In this case it is a good approximation to treat the phonon system as a phonon bath, neglecting effects related to coherent and nonequilibrium phonons. Furthermore, we will consider only the case of low temperatures where phonon absorption processes are negligible. Results for elevated temperatures will be published elsewhere.

Our main focus is the spatiotemporal dynamics of electrons and holes. Therefore we will extract from the single-particle density matrices the spatially resolved electron and hole densities according to

$$n^{e,h}(z,t)=\sum_{n',n}\varphi_{n'}^{e,h*}(z)\rho_{n',n}^{e,h}(t)\varphi_n^{e,h}(z). \tag{8}$$

For the interpretation of the results it will be particularly useful to study also the dynamics of the occupations of certain single-particle states. These occupations are given by the diagonal elements of the density matrices $\rho_{n,n}^{e,h}(t)$.

In the first part we present results of calculations made in a one-band model, where the wave packet is assumed to be generated locally in the vicinity of the dot. The generation process is not explicitly included; instead we use an initial condition which reflects the result of the optical excitation. Below we will show that for the present parameters this is a reasonable approximation. For the initial distribution we choose a Wigner function which factorizes into a Gaussian in position space [full width at half maximum (FWHM) 25 nm] and a Gaussian in the kinetic energy (mean energy 18 meV, FWHM 18 meV). This is chosen to mimic an optical generation by an ultrafast Gaussian laser pulse through the tip of a near-field microscope in the vicinity of the quantum dot. However, in $\mathbf{k}$ space we put the initial distribution only on one side of the energy parabola, where the momentum is directed toward the dot. We thus concentrate on the part of the electron wave packet moving toward the dot. The part of the wave packet that is moving away from the dot is obviously unimportant for studies of the capture process. This will be shown explicitly in the last part of this section where we account for the full k-symmetric carrier generation within a two-band model.

We will analyze the influence of weakly reflecting as well as strongly reflecting quantum dot potentials on the dynamics of the wave packet traveling in the quantum wire. The weakly reflecting quantum dot potential for the electrons $V^e(\mathbf{r})$ is modeled by

$$V^e(z)=-V_0\mathrm{sech}(z/a). \tag{9}$$

The parameters V_0 and a determine the depth and the width of the dot, respectively, and therefore the number and energies of the bound states. The strongly reflecting quantum dot potential will be modeled by a square well potential of depth V_0 and width a.

A. Weakly reflecting quantum dot potential: One bound level

First we will consider the case of a shallow, weakly reflecting potential [Eq. (9)] which is achieved by setting $V_0=30$ meV and $a=4$ nm. This quantum dot potential has one bound level at an energy of -14.4 meV. Figure 1 shows the electron density as a function of space and time for the cases (a) without and (b) with carrier-phonon interaction. The spatial profile of the initial distribution and the quantum dot potential are shown in the inset. Let us first concentrate on the case without carrier-phonon interaction. The wave packet starts 90 nm away from the dot center and begins to spread due to the dispersion. When the wave packet reaches the dot region (from about -20 to 20 nm), it splits because of the higher kinetic energy and the resulting higher group velocity of the front part of the wave packet above the dot. After the passage it reshapes again and no density remains in the dot region. Since the dot potential is sufficiently smooth there is almost no reflection of the wave packet in this case.

Figure 1(b) shows the electron dynamics including the interaction with longitudinal optical phonons, where the situation is completely different. Again, the wave packet moves toward the dot but now a considerable contribution of the density remains in the dot region. This clearly indicates a capture into the localized state of the dot by means of the emission of a LO phonon. In addition to this capture we notice another significant difference compared to the case without phonon interaction. We do not have just one transmitted wave packet but the initially transmitted wave packet is followed by a sequence of other smaller wave packets. This already indicates that the capture process when viewed at such short time and length scales exhibits pronounced differences compared to a process described simply by a semiclassical capture rate.

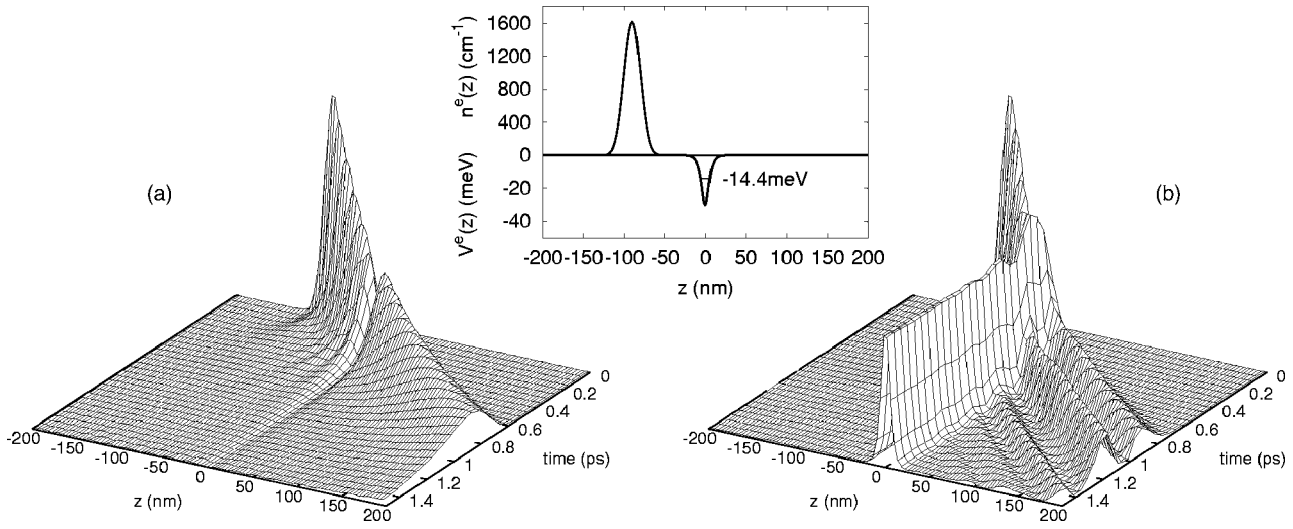

FIG. 1. Electron density in the one-band model as a function of space and time (a) without and (b) with carrier-phonon interaction. Inset: initial electron distribution and quantum dot potential in real space with one bound level at −14.4 meV.

To interpret the real space dynamics we have analyzed the occupations of the single-particle eigenstates. Figure 2(a) shows the occupation of the bound state as a function of time normalized to the total occupation of all states. We observe that the occupation remains essentially zero until about 200 fs when the wave packet reaches the dot region. Then the occupation exhibits a steep rise reflecting the capture of carriers from the continuum states to the bound state by means of phonon emission. However, the occupation does not rise monotonically as one would expect from a simple semiclassical capture rate but it exhibits an overshoot and pronounced oscillations until it finally reaches an asymptotic value of about 32%. The overshoot and the oscillations are clear signatures of quantum kinetics. They are a consequence of the fact that unlike in classical kinetics here a scattering process has a finite temporal duration. During the evolution a coherent superposition of an initial continuum electron state without a phonon and a final electron state with a phonon emitted builds up. Only with increasing time do the coherences decay and the semiclassically allowed transition survives. At short times, according to energy-time uncertainty also energy-nonconserving transitions are possible, which give rise to the initial overshoot in the occupation of the bound state.

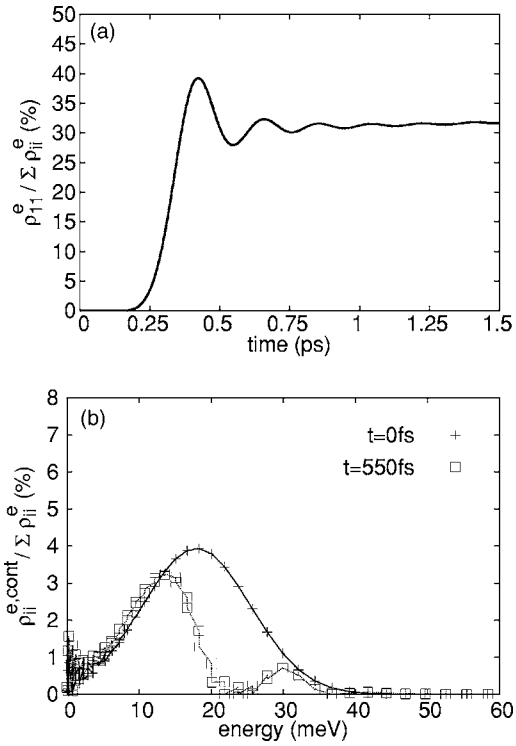

FIG. 2. (a) Occupation of the bound level at −14.4 meV as a function of time and (b) occupation of the continuum states at $t=0$ and 550 fs for the same scenario as in Fig. 1.

Characteristic for the present scenario is the fact that the spatial propagation of the carriers through the structured sample leads effectively to a temporal variation of the interaction between electrons and phonons. As long as the wave packet is in the quantum wire region we find some small effects due to a polaron dressing of the carriers which, however, leads only to small modifications of the wave packet dynamics when compared to the case without carrier-phonon interaction. As soon as the wave packet reaches the quantum dot region phonon emission becomes possible and, thus, the interaction is effectively switched on. If we had a single initial state and a single phonon mode this would lead to electron-phonon Rabi oscillations between the initial state without phonon and the final state with phonon, very similar to the case of atoms entering a microcavity where the switching on of the carrier-light interaction leads to electron-photon Rabi oscillations.[35] In our case we have a continuum of initial states and therefore a continuum of Rabi frequencies with variable detuning. This leads to a rather strong damping of the oscillations seen in Fig. 2(a). These Rabi-like oscillations also explain the emission of the follow-up wave packets. Whenever the system is in the continuum state without phonon there is a certain probability that the carriers leave the dot. Indeed, a close look at Fig. 1(b) reveals that the wave packets are always emitted when the occupation of the

ground state has a minimum. Since at low temperatures, as considered here, only phonon emission processes are possible, only coherences between initially occupied continuum states and the localized state build up. Thus, starting from continuum states with well-defined directions of their momenta, also after the completion of a full Rabi cycle only the initially occupied continuum states will be repopulated. This explains why the emitted wave packets always have the same direction as the initial wave packet. It should be mentioned that despite the qualitative analogy with atoms moving through a microcavity there are also several differences which prevent a direct quantitative comparison. Due to the broad continuum of energies here it is not justified to perform a rotating wave approximation as is usually done in quantum optics. Perfect Rabi oscillations, however, are only obtained within this approximation. Counter-rotating contributions lead to a coupling of the various transitions. In addition we have carrier-phonon coupling terms which are diagonal in the electron or hole states. These terms are also not present in the standard quantum optics models. Such a diagonal coupling gives rise to pure dephasing which is known to be the main source for the initial decoherence in strongly confined quantum dots.[34]

Figure 2(b) shows the occupations of the continuum states at two different times. The initial distribution ($t=0$) reflects the Gaussian Wigner distribution centered at 18 meV. Above a few meV the states are essentially plane waves and therefore the occupation of the eigenstates essentially agrees with the Wigner distribution. Only close to the band edge does the quantum dot potential modify the states resulting in some differences between the two pictures. The second curve ($t=550$ fs) refers to a time when the capture is nearly completed. We find a pronounced dip in the occupation at an energy of 22 meV which is exactly one LO phonon energy above the bound state. Thus, indeed the capture is most pronounced for the semiclassically allowed transition. But we also notice that there is a considerable broadening: the dip in the occupation has a width of several meV. This broadening reflects the energy-time uncertainty which cannot be neglected on these ultrafast time scales.

Since after the capture process a certain range of energies is missing in the continuum occupation, the question arises of what happens if the transmitted wave packet reaches another quantum dot. This is shown in Fig. 3 where the spatial electron density profile is plotted at different times for the case of two quantum dots separated by 100 nm. Due to the large distance between the dots they are effectively uncoupled and have quasidegenerate bound states. Figure 4 shows the corresponding time-resolved occupations of the ground states of the two quantum dots. For the first dot centered at −50 nm we observe the same behavior as discussed above: The capture starts at about 200 fs, the ground-state occupation exhibits an oscillatory behavior, and it reaches about 32%. The second dot is reached by the transmitted wave packet at about 500 fs. Subsequently, a transient occupation of the bound state of this dot builds up although we know that there is essentially no occupation in the continuum states about one LO phonon energy above the bound state. This is again a typical quantum kinetic feature related to energy time uncertainty. At $t=700$ fs we observe a clear peak

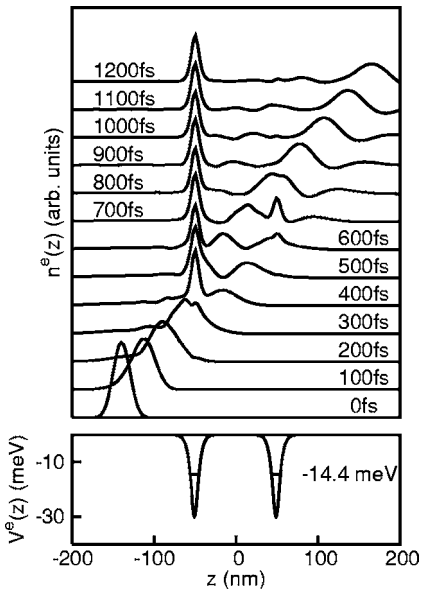

FIG. 3. Spatially resolved electron density at different times for the case of an electron wave packet approaching two identical quantum dot potentials. The lower part shows the double quantum dot potential with effectively uncoupled bound states of the dots at −14.4 meV.

in the spatially resolved profiles at the position of the second dot (cf. Fig. 3). After about 850 fs, however, most of this occupation has disappeared and only a few percent occupation is remaining. In Fig. 3 we only see the electrons trapped in the first dot as well as the outgoing wave packet leaving the regions of the quantum dots.

B. Weakly reflecting quantum dot: Three bound levels

The quantum dots studied so far were characterized by a single bound state. Let us now consider the case of a quantum dot potential with more than one bound state. To concentrate on the capture we choose again a sufficiently smooth potential to minimize reflection of the incident wave packet. Therefore we take again a potential of the form of Eq. (9), but now with the parameters $V_0=40$ meV and $a=10$ nm. This potential has three bound states at energies of −30.6, −15.2, and −5.8 meV. The initial conditions for the wave

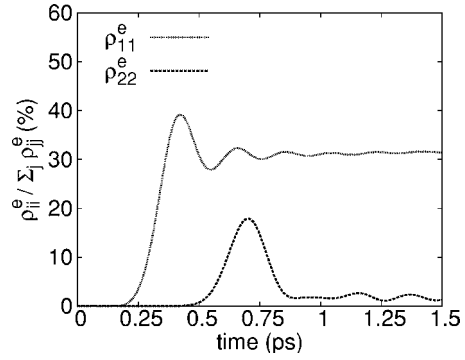

FIG. 4. Occupation of the bound levels in the two quantum dots of Fig. 3 as a function of time.

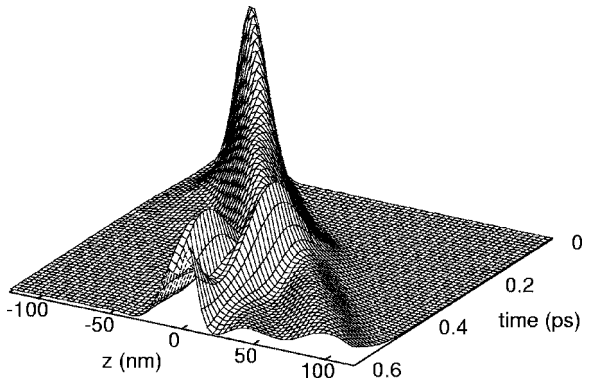

FIG. 5. Electron density as a function of space and time for the case of an electron wave packet approaching a quantum dot potential with three bound states.

packet are the same as in the previous case. Figure 5 shows the corresponding electron density as a function of space and time. We see again the initial wave packet approaching the quantum dot, the transmitted wave packet, and a part which remains localized around $z=0$, i.e., in the region of the quantum dot. If we compare this result with the result for the quantum dot with one bound level, we notice an interesting additional feature: The trapped wave packet has now a two-peak structure and the occupation oscillates between these two peaks. This is even more clearly visible in Fig. 6 where the spatial profiles of the electron distribution at different times are plotted for the cases without (dotted lines) and with (solid lines) electron-phonon interaction. Without interaction, as in the case of one bound state the wave packet exhibits some distortions in the region of the quantum dot but afterwards it reshapes and it is essentially completely transmitted.

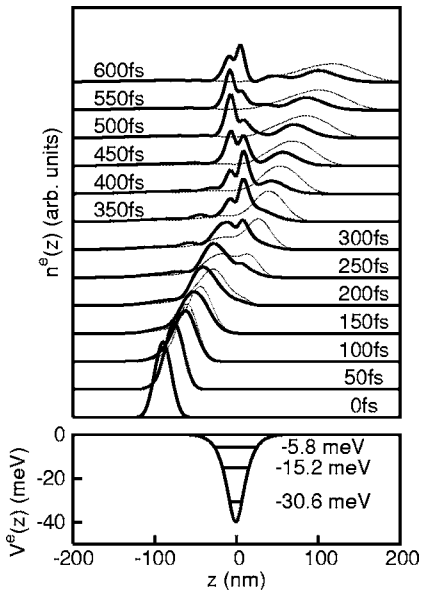

FIG. 6. Spatial profile of the electron density at different times for the case of a quantum dot potential with three bound states; dotted lines are without and solid lines with electron-phonon interaction. The lower part shows the potential profile together with the energies of the bound states.

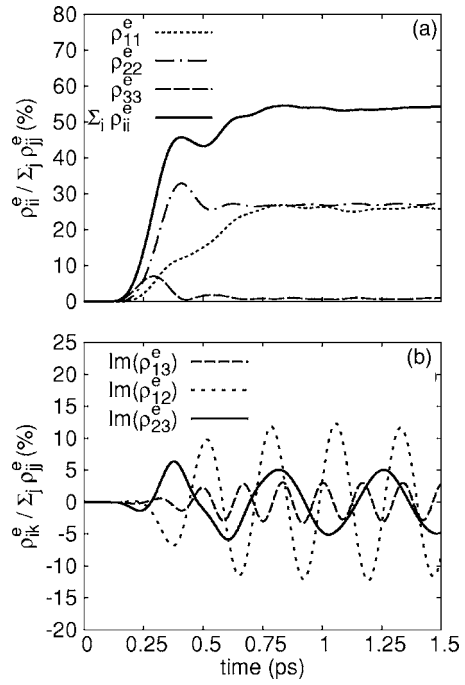

FIG. 7. (a) Occupations of the bound levels as functions of time (level 1, −30.6 meV; level 2, −15.2 meV; level 3, −5.8 meV) and (b) imaginary part of the coherences between the bound levels.

With carrier-phonon interaction switched on we see the oscillating double peak structure of the trapped carrier density. Obviously the trapped carrier density initially tries to follow the incoming wave packet until it reaches the right border of the quantum dot. There it is reflected and it starts to perform spatial oscillations inside the dot.

To understand this dynamical behavior let us look again at the occupations of the bound states. The individual occupations as well as the sum over all three bound states are plotted in Fig. 7(a) as a function of time. Again, the occupations start to grow at about 200 fs when the wave packet reaches the quantum dot. Interestingly we find that first the occupation of the third level starts to grow, then that of the second level, and finally the occupation of the lowest level. This can be understood from the spatial structure of the bound states. The deeper the energy of the bound state the more localized is the wave function. Therefore the traveling wave packet first overlaps with the highest, i.e., the third, state. This transition, however, is far off resonance and therefore the occupation is only transient. The second state is closest to resonance. Its occupation exhibits a dynamical behavior similar to the case of a single bound state as studied above. After some oscillations it reaches an asymptotic value of about 27%. The transition to the lowest state at −30.6 meV is resonant for the carriers close to the band edge. These carriers are quite slow and therefore the occupation grows much more slowly than for the second state where the carriers in the initial state move much faster. In total we find a capture efficiency of about 55%.

The dynamics of the occupations, however, does not yet explain the oscillations found in the trapped density. Their origin becomes clear when looking at the off-diagonal elements of the density matrix in the subspace of the bound

states. The imaginary parts of these coherences between all pairs of the three bound states are plotted as a function of time in Fig. 7(b). Like the diagonal elements they have been normalized to the total occupation. The real parts exhibit a similar behavior and are therefore not shown here. We find that after about 200 fs all off-diagonal elements are nonvanishing and they exhibit a periodic oscillation. The period of the oscillation of the variable ρ_{ij} agrees with the Bohr period of the transition $2\pi\hbar/(\epsilon_i-\epsilon_j)$. The presence of these off-diagonal elements demonstrates the fact that after the capture process the carriers do not simply occupy with a certain probability one of the bound states; instead they are in a coherent superposition of these states. We find a particularly pronounced coherence between the ground state and the first excited state where the off-diagonal elements are indeed of the same order of magnitude as the diagonal elements. This coherent superposition of the symmetric ground state with the antisymmetric first excited state gives rise to the spatial oscillations of the trapped wave packet observed in Figs. 5 and 6. These oscillations are therefore a typical quantum mechanical effect and would not be present in any calculation based on a semiclassical capture rate.

The creation of coherent superposition states in an interaction process shows again strong analogies between carrier-phonon and carrier-light interaction. As already mentioned, due to the motion of the traveling wave packet across the quantum dot region the carrier-phonon interaction is active only during a certain time interval. From the wave packet dynamics without carrier-phonon interaction in Fig. 6 we can extract an effective interaction time of about 200 fs which also agrees with the rise time of the occupation of the second level in Fig. 7. This time is shorter than the Bohr period of the most important coherence between the ground and the first excited state which is 270 fs. Therefore the situation is similar to the case of the interaction with a short laser pulse where also quantum beats between different states are excited if the pulse spectrum overlaps with two or more transitions or, equivalently, if the pulse duration is shorter than the Bohr periods corresponding to the energy differences of the transitions involved.

C. Strongly reflecting quantum dot

In the previous sections we have discussed smooth quantum dot potentials. In those cases the incoming electron wave packet has been partly captured into the localized states of the dot while the remaining part was transmitted through the dot region. As soon as there are sharp potential variations there appears a third possibility, the reflection of the incoming carrier distribution. A typical example where such a behavior occurs is a square well potential. Therefore, in this section we study the carrier capture processes in the case of a square well potential with a depth of −25 meV and a width of 30 nm. This dot has two bound states at energies of −11.2 and −21.4 meV. We will compare an initial condition where the incoming wave packet is located in a reflection maximum with the case where the energy of the wave packet is centered at a transmission maximum. For the potential profile chosen here the first reflection maximum is at an energy of

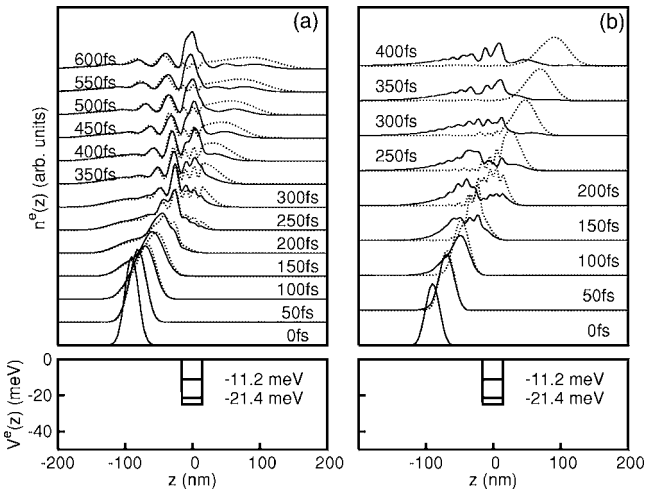

FIG. 8. Spatial profiles of the electron density at different times for the case of an electron wave packet approaching a square well potential. (a) refers to an initial excess energy of 12 meV (reflection maximum) and (b) to an excess energy of 34 meV (transmission maximum). The dotted lines are without and the solid lines with carrier-phonon interaction.

12 meV with a reflection probability of about 25%. The next transmission maximum is then at 34 meV. Therefore, as initial conditions we have chosen Gaussian kinetic energy distributions centered around these two values and, as in the previous cases, with a FWHM of 18 meV. The spatial profiles of the electron distribution at different times for these two initial conditions are plotted in Fig. 8. The left panel refers to the injection at the reflection maximum while the right panel corresponds to the transmission maximum. In both cases the dotted lines are the results of calculations without carrier-phonon interaction and the solid curves are the results including carrier-phonon interaction. Let us first discuss the results without this interaction. In Fig. 8(a) the wave packet approaches the dot. Then, due to reflections at the two interfaces between quantum dot and surrounding material a standing wave pattern builds up inside the dot region and finally a part of the wave packet is transmitted while another part is reflected. This reflected wave packet interferes with the slow parts of the incoming wave packet which results in the oscillatory density profiles at negative values of z. Due to the absence of carrier-phonon interaction there is essentially no electron density remaining in the region of the quantum dot. In the case of injection at the transmission maximum [dotted line in Fig. 8(b)] we again observe the buildup of the standing wave pattern in the quantum dot, but at later times the wave packet reshapes and it is nearly completely transmitted through the quantum dot region.

Let us now come to the cases with carrier-phonon interaction switched on (solid curves in Fig. 8). We first notice that for both initial conditions now there is a considerable part of the electron density remaining in the quantum dot region indicating the carrier capture. The trapped carrier density exhibits a one peak structure in Fig. 8(a) while in Fig. 8(b) it is characterized by a two-peak structure. This different behavior can be understood from Fig. 9, where we have plotted the occupations and coherences of the bound states for

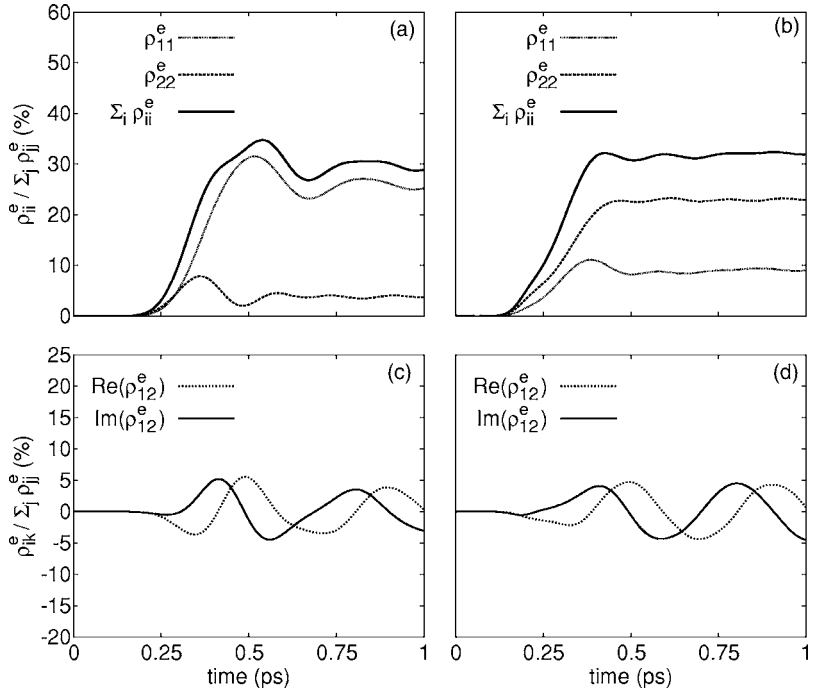

FIG. 9. (a), (b) Occupations of the bound states and (c), (d) coherences between these states as a function of time for the case of a square well potential. The left part (a), (c) refers to an initial energy of 12 meV (reflection maximum), the right part (b), (d) to an initial energy of 34 meV (transmission maximum).

the present scenarios. Indeed, for carriers incident at the reflection maximum [Figs. 9(a) and 9(c)] the capture mainly results in an occupation of the ground state with only a small occupation of the excited state. This is because the incident energy is roughly one LO phonon energy above the ground state such that this transition is close to resonance. The ground-state wave function is an even function without a node which explains the single-peak structure in the trapped density profile. For the case of injection at the transmission maximum [Figs. 9(b) and 9(d)] the initial energy is much higher and the transition to the excited state is much closer to resonance than the ground-state transition. Therefore, now the excited state is mainly populated; it has an odd wave function with a node in the center and thus gives rise to the two-peak structure of the trapped density.

When comparing the results with and without carrier-phonon interaction in Fig. 8 we notice another interesting feature. When injecting at the reflection maximum the reflected part is nearly unchanged by the capture. Essentially all of the trapped carriers are taken from the transmitted wave packet which is considerably reduced compared to the case without electron-phonon interaction. A different behavior is observed in the case of injection at the transmission maximum. Without carrier-phonon interaction there is essentially only transmission; therefore this part has to be reduced when capture processes occur. However, in addition to the capture we now find also a considerable enhancement of the reflected contribution. Thus we find that the presence of an inelastic channel (the emission of LO phonons) also modifies the elastic scattering properties of the potential profile. This can be traced back to two basic phenomena. First the presence of carrier-phonon interaction in a quantum kinetic calculation slightly modifies the spectral properties of the quasiparticles. Instead of electrons we now deal with polarons with a slightly changed effective mass and ground state energy. This renormalization leads to a shift of the position of transmission or reflection maxima. In the present case this is of minor importance because these maxima are relatively broad. Second and more important, as is well known from a Fabry-Pérot resonator, the perfect transmission at a certain energy is a result of the perfect destructive interference of all waves which are reflected at the two boundaries. The presence of an inelastic channel modifies the phases of the wave functions and therefore destroys the condition of exact destructive interference resulting in a finite reflection at this energy.

D. Capture in the two-band model

Up to now we have discussed the results obtained within a one-band model. This has allowed us to concentrate on the electronic capture process and in particular to analyze the pertinent quantum features in such processes which are a consequence of the ultrashort length and time scales. In these calculations we started with a given initial distribution. Of course, for a realistic modeling it is necessary to specify how such an initial condition could be realized. As already mentioned in the introduction, a carrier distribution that is localized both in real space and momentum space could be achieved by an optical excitation of an intrinsic semiconductor with a strongly focused laser pulse, e.g., by means of excitation through the tip of a near-field microscope.[14,16] In the present section we include explicitly this generation process. Now the electron-phonon system is initially in the well-defined vacuum state. The laser pulse is modeled by a transverse electric field which is Gaussian in space and time and is coupled to the semiconductor by means of the usual dipole coupling.[16] We thus neglect possible effects of longitudinal evanescent fields of the near-field tip. Such fields are known to become important very close to the tip. Typically they are of minor importance if there is some kind of spacer between the tip and the semiconductor nanostructure, in our case, e.g.,

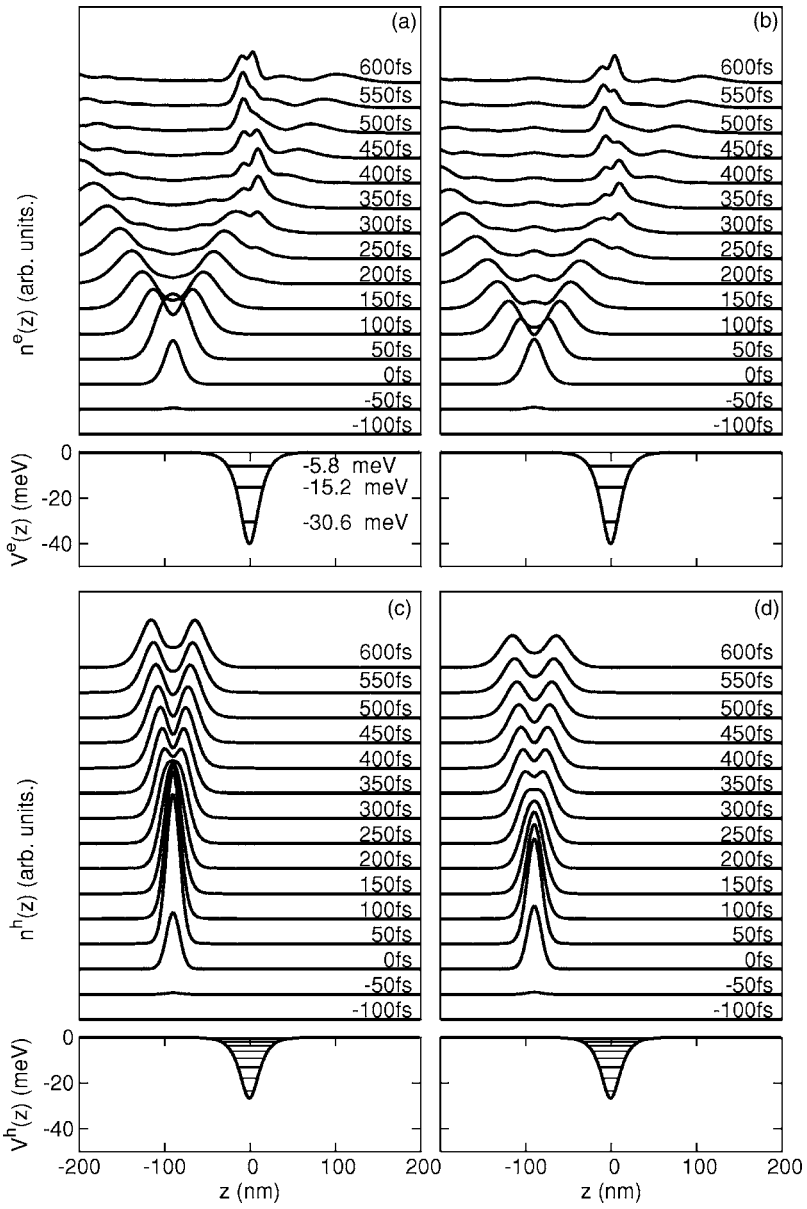

FIG. 10. Spatial profiles of the (a), (b) electron and (c), (d) hole density at different times for the case of a quantum dot potential with three bound states obtained from simulations within a two band model. The left part refers to a calculation without Coulomb interaction; in the right part Coulomb interaction has been included on the mean-field level (time-dependent Hartree-Fock approximation).

a barrier material around the quantum wire. It is well known that the optical properties of semiconductors in particular in the vicinity of the band gap are strongly determined by Coulomb effects.[2] Therefore in the following we will compare calculations performed without Coulomb interaction with calculations where this interaction has been included on the mean-field level and which, therefore, fully account for the presence of an excitonic absorption as well as Coulomb-induced modifications of the oscillator strengths of optical transitions in the band-to-band continuum.

To be comparable with the one-band calculations we have chosen the same potential profile for the electrons as in Sec. III B, i.e., a weakly reflecting potential supporting three bound states. Assuming a valence band discontinuity of 2/3 of the electron discontinuity as well as standard GaAs material parameters, this leads to a quantum dot potential for the holes with seven bound states which, however, will not be important in the following. To model the optical excitation we use a 50 fs laser pulse with an excess energy of 20 meV centered at $t=0$ and a Gaussian spatial distribution centered at $z=-90$ nm with a FWHM of 25 nm. The resulting spatial profiles of electrons and holes at different times are plotted in Fig. 10. Here the left panel refers to the calculations without Coulomb interaction while in the right panel this interaction has been included on the mean-field (time-dependent Hartree-Fock) level. Around $t=0$ we see the generation of the electron and hole distributions. The electron distribution starts to separate into a left- and a right-moving wave packet already during the excitation process. The holes, because of their much smaller group velocities, separate into two wave packets only at much later times. Because of these slow velocities they do not reach the quantum dot within the simulation time and therefore we do not observe hole trapping in the present case. The most obvious difference in the electron dynamics compared to the one-band calculations (see Fig. 6) is the presence of two wave packets moving in opposite directions. This is because the coupling to the light field is symmetric with respect to k and therefore does not lead to a

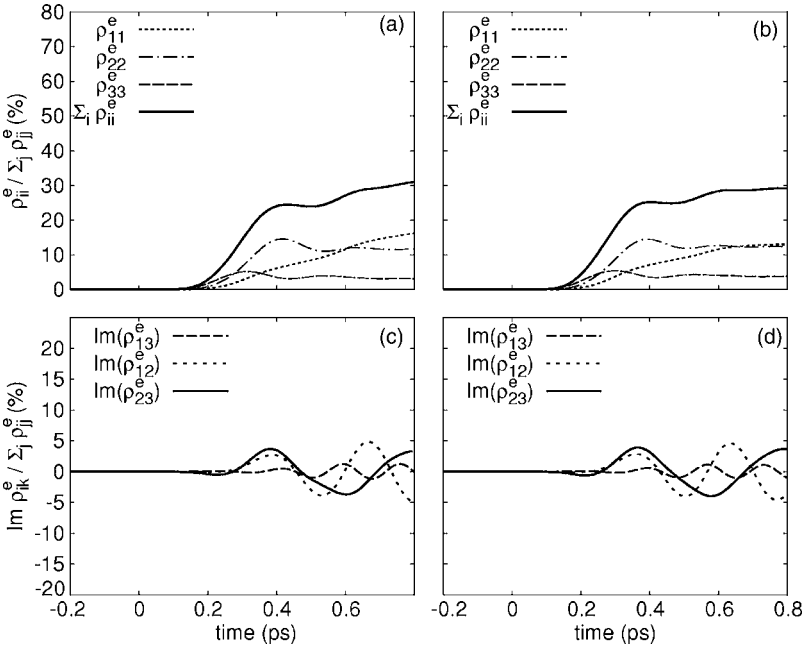

FIG. 11. (a), (b) Occupations of the bound electron states and (c), (d) coherences between the bound electron states obtained from simulations within a two-band model. The left part refers to a calculation without Coulomb interaction; in the right part the Coulomb interaction has been included on the mean-field level.

preferential direction. But the results also show that the wave packet moving away from the quantum dot does not influence the capture dynamics, therefore it was justified to concentrate on a wave packet moving in one direction in the one band calculations. Also the trapping dynamics is very similar to the one-band case. In Fig. 10 we again find a two-peak structure and spatial oscillations of the trapped electron distribution very similar to Fig. 6. This is also confirmed by Fig. 11 where we have plotted the occupations and coherences of the bound electron states in the two-band case. The most pronounced difference compared to Fig. 7 is the reduction of all variables roughly by a factor of 2. This is simply due to the presence of the wave packet moving away from the dot which contributes to the total carrier density and therefore to the normalization of the density matrix elements. Some small quantitative differences are related to the fact that the coherent generation process with a pulse of finite duration does not lead exactly to the same initial distribution as used in the one band calculations. It has been found earlier[21] that in a quantum kinetic model we find a somewhat enhanced occupation at higher energies which is probably the reason for the somewhat larger occupation of the third state in the two-band calculations.

Interestingly we find only small differences between the calculations with and without Coulomb interaction. The reason is that obviously the excess energy of 20 meV is already sufficient to essentially remove excitonic effects. Nevertheless there are a few Coulomb-related features observable. First of all, the total number of electron-hole pairs which is generated by a laser pulse of given field amplitude is reduced if the Coulomb interaction is switched on, as can be seen most clearly in the hole density profiles in Fig. 10. This is a consequence of the Coulomb-induced modifications of the oscillator strengths of interband transitions which in a quantum wire leads to a reduction of the absorption above the band gap[36] in contrast to two- and three-dimensional systems where the absorption is enhanced.[37] Second, we find that the occupation of the ground state is smaller in the calculations with Coulomb interaction than without this interaction. This can again be attributed to the reduction of the absorption above the band gap in quantum wires which completely removes the singularity at the band edge typical for one-dimensional systems. As already mentioned in Sec. III B, the ground state is mainly populated from carriers close to the band edge because this transition is close to resonance. Therefore, the effective reduction of the density of states in this energy window also reduces the capture processes from these states. Finally, when looking at the electron density profiles in Fig. 10(b) we observe a small peak which remains localized at the position of the generation. These are electrons which are bound in excitons with vanishing center-of-mass momentum. Since the exciton line in the absorption spectrum is very strong, the small spectral overlap of the exciting pulse with this line is still sufficient to produce a small but clearly observable number of excitons. The formation of bound excitons from electron-hole pairs excited in the continuum below the threshold for LO phonon emission due to the interaction with acoustic phonons occurs on a much longer time scale and need not to be taken into account here.[38] Besides these three phenomena, the reduction of the total density, a somewhat reduced occupation of the ground state, and a small excitation of bound excitons, the capture process turns out to be essentially not affected by the mean-field Coulomb terms.

IV. CONCLUSIONS

In this paper we have presented a detailed analysis of the ultrafast dynamics of carrier capture processes in semiconductor nanostructures due to the polar interaction with LO phonons. Our calculations have been based on a quantum kinetic density matrix approach for both a one-band and a two-band model. The former allowed us to concentrate on the capture process of a single species of carriers; within the

latter we then have included the optical excitation process as well as the Coulomb interaction in mean-field approximation which allowed us to realistically model a scenario which at least in principle is experimentally accessible.

Our results showed that on the ultrashort length and time scales considered here there are plenty of deviations from the simple semiclassical picture of a capture process described by a capture rate. At low temperatures where phonon absorption processes are absent such a capture rate would always lead to a monotonic rise of the occupation of bound states. In contrast, we have found already in the simplest case of a smooth quantum dot potential with a single bound state that the occupation exhibits a nonmonotonic rise including an overshoot and subsequent oscillations. The overshoot is the result of energy-time uncertainty. The oscillations can be interpreted as carrier-phonon Rabi oscillations between a continuum state without phonon and a localized state with phonon which are excited due to the effective switching on of the carrier-phonon interaction when the wave packet reaches the quantum dot region.

The capture process exhibits additional interesting features in the case of quantum dot potentials with more than one bound state. In this case we have found that in general the capture does not simply lead to certain occupations of the bound states but that linear superpositions of these bound states are populated. These superpositions then give rise to a nontrivial spatiotemporal dynamics of the trapped carrier density, e.g., in the case of a superposition between states with even and odd symmetry to spatial oscillations inside the quantum dot. The creation of these superposition states can be understood from the effectively finite duration of the carrier-phonon interaction which is active only as long as the traveling wave packet is in the dot region.

If the quantum dot potential exhibits sharp discontinuities as in the case of a square well potential, besides transmission and capture there is also the possibility of reflection of the incident wave packet. We have found that the inelastic carrier capture process may have a pronounced effect on the reflection and transmission characteristics. Because it affects the phase of the wave packet dynamics it can remove the conditions for perfect destructive interference of the reflected parts and thereby considerably enhance the reflection probability.

We have then extended our studies to the more realistic two-band model including the coherent carrier generation process and excitonic effects. We found some quantitative differences compared to the one-band calculations but remarkably little influence on the dynamics of the capture process. In particular the capture into superposition states associated with spatial oscillations of the trapped electron density are almost the same as in the one-band case. Therefore the use of the numerically simpler one-band model for the study of the kinetics of capture processes at least under the present excitation conditions is well justified. But, of course, as soon as optical signals have to be calculated, for example to interpret spatially resolved pump-probe experiments,[16] a two-band model is necessary.

The strong deviations from the semiclassical picture reported here for the ultrafast dynamics of capture processes directly reflects the memory structure inherent in the quantum kinetic treatment. Our results reveal a variety of interesting phenomena which become accessible when the quantum kinetic regime is reached. Moreover, the phase sensitivity that is characteristic for such memory effects may open perspectives to manipulate the interacting dynamics when the system is probed on ultrashort time and length scales.

ACKNOWLEDGMENTS

This work has been partially supported by the Deutsche Forschungsgemeinschaft through the Graduiertenkolleg Nichtlineare kontinuierliche Systeme and the Schwerpunktprogramm Quantenkohärenz in Halbleitern.

[1] H. Haug and A.-P. Jauho, *Quantum Kinetics in Transport and Optics of Semiconductors* (Springer, Berlin, 1998).
[2] V. M. Axt and T. Kuhn, Rep. Prog. Phys. **67**, 433 (2004).
[3] W. Wegscheider, G. Schedelbeck, G. Abstreiter, M. Rother, and M. Bichler, Phys. Rev. Lett. **79**, 1917 (1997).
[4] C. Lienau, V. Emiliani, T. Guenther, F. Intonti, T. Elsaesser, R. Nötzel, and K. H. Ploog, Phys. Status Solidi A **178**, 471 (2000).
[5] H. Shichijo, R. M. Kolbas, N. Holonyak, R. D. Dupuis, and P. D. Dapkus, Solid State Commun. **27**, 1029 (1978).
[6] J. A. Brum and G. Bastard, Phys. Rev. B **33**, 1420 (1986).
[7] T. Kuhn and G. Mahler, Solid-State Electron. **32**, 1851 (1989).
[8] P. W. M. Blom, C. Smit, J. E. M. Haverkort, and J. H. Wolter, Phys. Rev. B **47**, 2072 (1993).
[9] M. Preisel and J. Mørk, J. Appl. Phys. **76**, 1691 (1994).
[10] R. Ferreira and G. Bastard, Appl. Phys. Lett. **74**, 2818 (1999).
[11] I. Magnusdottir, S. Bischoff, A. V. Uskov, and J. Mørk, Phys. Rev. B **67**, 205326 (2003).
[12] A. Markus and A. Fiore, Phys. Status Solidi A **201**, 338 (2004).
[13] T. R. Nielsen, P. Gartner, and F. Jahnke, Phys. Rev. B **69**, 235314 (2004).
[14] V. Emiliani, T. Günther, F. Intonti, A. Richter, C. Lienau, and T. Elsaesser, J. Phys.: Condens. Matter **11**, 5889 (1999).
[15] U. Neuberth, L. Waller, G. von Freymann, B. Dal Don, H. Kalt, M. Wegener, G. Khitrova, and H. M. Gibbs, Appl. Phys. Lett. **80**, 3340 (2002).
[16] T. Guenther, C. Lienau, T. Elsaesser, M. Glanemann, V. M. Axt, T. Kuhn, S. Eshlaghi, and A. D. Wieck, Phys. Rev. Lett. **89**, 057401 (2002).
[17] A. Naber, D. Molenda, U. C. Fischer, H.-J. Maas, C. Höppener, N. Lu, and H. Fuchs, Phys. Rev. Lett. **89**, 210801 (2002).
[18] F. Steininger, A. Knorr, T. Stroucken, P. Thomas, and S. W. Koch, Phys. Rev. Lett. **77**, 550 (1996).
[19] B. Hanewinkel, A. Knorr, P. Thomas, and S. W. Koch, Phys. Rev. B **60**, 8975 (1999).
[20] F. Steininger, A. Knorr, P. Thomas, and S. W. Koch, Z. Phys. B: Condens. Matter **103**, 45 (1997).

[21] M. Herbst, M. Glanemann, V. M. Axt, and T. Kuhn, Phys. Rev. B **67**, 195305 (2003).
[22] M. Herbst, V. M. Axt, and T. Kuhn, Phys. Status Solidi B **221**, 419 (2000).
[23] F. Rossi and T. Kuhn, Rev. Mod. Phys. **74**, 895 (2002).
[24] D. B. Tran Thoai and H. Haug, Phys. Rev. B **47**, 3574 (1993).
[25] C. Fürst, A. Leitenstorfer, A. Laubereau, and R. Zimmermann, Phys. Rev. Lett. **78**, 3733 (1997).
[26] M. Betz, G. Göger, A. Laubereau, P. Gartner, L. Bányai, H. Haug, K. Ortner, C. R. Becker, and A. Leitenstorfer, Phys. Rev. Lett. **86**, 4684 (2001).
[27] V. M. Axt, M. Herbst, and T. Kuhn, Superlattices Microstruct. **26**, 117 (1999).
[28] R. Huber, C. Kübler, S. Tübel, A. Leitenstorfer, Q. T. Vu, H. Haug, F. Köhler, and M.-C. Amann, Phys. Rev. Lett. **94**, 027401 (2005).
[29] P. Gartner, L. Bányai, and H. Haug, Phys. Rev. B **62**, 7116 (2000).
[30] T. Wolterink, V. M. Axt, and T. Kuhn, Phys. Rev. B **67**, 115311 (2003).
[31] J. Schilp, T. Kuhn, and G. Mahler, Semicond. Sci. Technol. **9**, 439 (1994).
[32] L. Besombes, K. Kheng, L. Marsal, and H. Mariette, Phys. Rev. B **63**, 155307 (2001).
[33] A. Vagov, V. M. Axt, T. Kuhn, W. Langbein, P. Borri, and U. Woggon, Phys. Rev. B **70**, 201305(R) (2004).
[34] B. Krummheuer, V. M. Axt, and T. Kuhn, Phys. Rev. B **65**, 195313 (2002).
[35] J. M. Raimond, M. Brune, and S. Haroche, Rev. Mod. Phys. **73**, 565 (2001).
[36] F. Rossi and E. Molinari, Phys. Rev. Lett. **76**, 3642 (1996).
[37] H. Haug and S. W. Koch, *Quantum Theory of the Optical and Electronic Properties of Semiconductors* (World Scientific, Singapore, 1993).
[38] K. Siantidis, V. M. Axt, and T. Kuhn, Phys. Rev. B **65**, 035303 (2002).